The E2 Ubiquitin Conjugating Enzyme UBE2J1 is Required for Spermiogenesis in Mice

Paul-Albert Koenig[1], Peter K. Nicholls[1], Florian I. Schmidt[1], Masatoshi Hagiwara[1], Takeshi Maruyama[1], Galit H. Frydman[2], Nicki Watson[1], David C. Page[1,3,4], Hidde L. Ploegh[1,3]

[1] Whitehead Institute for Biomedical Research, Cambridge, MA 02142, USA
[2] Division of Comparative Medicine, Massachusetts Institute of Technology, Cambridge, MA 02139, USA
[3] Department of Biology, Massachusetts Institute of Technology, Cambridge, MA 02142, USA
[4] Howard Hughes Medical Institute, Cambridge, MA 02142, USA

*Running title: *Male Ube2j1$^{-/-}$ mice are sterile*

To whom correspondence should be addressed: Hidde Ploegh, Whitehead Institute for Biomedical Research, 9 Cambridge Center, Cambridge 02142, MA, USA, Tel.: +1-617-324-2031; Fax: +1-617-452-3566; e-mail: ploegh@wi.mit.edu

Keywords: ER quality control, endoplasmic‐reticulum‐associated protein degradation (ERAD), ubiquitin‐conjugating enzyme (E2 enzyme), gene knockout, spermatogenesis, mouse model, male infertility, spermiogenesis, ERAD tuning

Background: The physiological roles of many ER quality control components are unknown.
Results: Male *Ube2j1*$^{-/-}$ mice are sterile with defects in flagella and acrosome function, and cytoplasm removal in sperm cells.
Conclusion: Spermatogenesis is a previously unknown process requiring ER quality control.
Significance: ER quality control components might serve as diagnostic or therapeutic targets for male infertility in the future.

ABSTRACT

ER-resident proteins destined for degradation are dislocated into the cytosol by components of the ER quality control machinery for proteasomal degradation. Dislocation substrates are ubiquitylated in the cytosol by E2 ubiquitin conjugating/E3 ligase complexes. UBE2J1 is one of the well-characterized E2 enzymes that participate in this process. However, the physiological function of *Ube2j1* is poorly defined. We find that *Ube2j1*$^{-/-}$ mice have reduced viability and fail to thrive early after birth. Male *Ube2j1*$^{-/-}$ mice are sterile due to a defect in late spermatogenesis. Ultrastructural analysis shows that removal of the cytoplasm is incomplete in *Ube2j1*$^{-/-}$ elongating spermatids, compromising the release of mature elongate spermatids into the lumen of the seminiferous tubule. Our findings identify an essential function for the ubiquitin-proteasome-system in spermiogenesis and define a novel, non-redundant physiological function for the dislocation step of ER quality control.

Components of the endoplasmic reticulum (ER) quality control system recognize proteins no longer wanted in the ER and target them for degradation. During this process, misfolded proteins are extracted from the ER (ER dislocation) and delivered to the cytosol for proteasomal degradation (1). Substrate dislocation is driven by concerted ubiquitylation and deubiquitylation reactions (2). Ubiquitylation involves the action of three enzymes, E1 ubiquitin-activating enzymes, E2 ubiquitin-conjugating enzymes, and E3 ubiquitin ligases.

E2 ubiquitin-conjugating enzymes known to be involved in ER dislocation include the yeast Ubc6p orthologs UBE2J1 (UBC6e, NCUBE1) and UBE2J2 (UBC6, NCUBE2) (3,4), tail-anchored proteins in the ER membrane with their catalytic domain facing the cytosol. UBE2J1 is part of the SEL1L dislocation complex, which contains several other factors known to be involved in ER dislocation. These include HRD1, Derlin-2, p97, PDI, BiP, Calnexin, AUP1, UBXD8 and OS9 (5).

In the absence of β2-microglobulin, the heavy chain of the human class I MHC molecule HLA-B27 is ubiquitylated, dislocated and degraded by the concerted action of UBE2J1 and the E3 ligase HRD1 (Synoviolin) (5). In contradistinction, UBE2J1 cooperates with the E3 ligase RMA8 and with Derlin-1 in the degradation of CFTRΔ508 (6). Moreover, UBE2J1 is involved in the degradation of other model substrates for ER dislocation, such as the unpaired TCRα chain, and class I MHC heavy chains in the presence of the HCMV-derived immunoevasin US11 (4,6).

Despite accumulating data in tissue culture models on the function and mechanisms of ER dislocation, its physiological function in an organismal context is poorly defined, due to the limited number of model substrates and cell lines investigated and due to the lack of appropriate *in vivo* mammalian models. To obtain further insight into the physiological role of ER dislocation, we generated a floxed allele of *Ube2j1* in mice and analyzed *Ube2j1*$^{-/-}$ mice.

Although *Ube2j1* has been repeatedly implicated in the dislocation of various misfolded glycoprotein substrates, mice that lack *Ube2j1* are viable and show no gross aberrations in morphology or behavior. On the assumption that ER quality control is essential to development and survival, these results suggest remarkable redundancy in its mode of operation. The main defect we observe in *Ube2j1*$^{-/-}$ animals, surprisingly, is male sterility due to defects in flagella and acrosome function, and defective removal of cytoplasm from elongating spermatids. Our results thus identify a unique, non-redundant role for *Ube2j1* in male germ cell development and define a previously unknown physiological function of ER dislocation.

EXPERIMENTAL PROCEDURES

Generation of Ube2j1$^{fl/fl}$ mice - We generated mice carrying a conditional allele of the gene encoding UBE2J1 (also known as UBC6e or NCUBE1, gene name *Ube2j1*) by homologous recombination (Fig. 1A). Genomic sequences were amplified by PCR from a BAC clone (Clone DB name RP24-531A22; C57BL/6J, male, brain, spleen; BAC-PAC Resources, Oakland, CA) containing the genomic sequence of *Ube2j1* from C57BL/6J mice. *Ube2j1* consists of 8 exons. We constructed a targeting vector based on the pPGKneoF2L2dta ('pF2L2', Addgene 13445, (7)) vector to install LoxP sites in introns 1 and 3, allowing conditional ablation of *Ube2j1* in the presence of Cre recombinase. A neomycin resistance cassette flanked by FRT sites was inserted upstream of the 3' LoxP site between exon 3 and 4. The LoxP sites were flanked by a ~4.6 kb 5' and a ~2.8 kb 3' homology arm. The linearized targeting construct was electroporated into JM8A3.N1 ES cells (strain C57BL/6N, agouti; obtained from the KOMP Repository), which were subsequently grown in the presence of neomycin. ES cells were selected with 300 μg/mL G418 (Geneticin; Gibco, Life Technologies; Grand Island, NY) for six days. G418-resistant ES cell colonies were screened for correct targeting by Southern blotting or long range PCR, and correctly targeted ES cell clones were injected into C57BL/6J blastocysts. Chimeras were bred with FLPe transgenic mice (JAX strain B6.Cg-Tg(ACTFLPe)9205Dym/J; Jackson Laboratories, Bar Harbor, ME) to excise the neomycin resistance cassette. Ube2j1$^{fl/WT}$ mice were intercrossed to obtain FLPe^{-} *Ube2j1*$^{fl/WT}$ mice. FLPe^{-} *Ube2j1*$^{fl/WT}$ mice were then crossed to CMV-Cre transgenic mice (JAX strain B6.C-Tg(CMV-cre)1Cgn/J; Jackson Laboratories, Bar Harbor, ME) to generate full-body knockout mice (*Ube2j1*$^{-/-}$) and to CD19-Cre mice (JAX strain B6.129P2(C)-*Cd19tm1(cre)Cgn*/J; Jackson Laboratories, Bar Harbor, ME) for specific ablation in B cells (CD19-Cre *Ube2j1*$^{fl/fl}$).

Mice were genotyped by PCR using primers annealing to the genomic regions indicated in Fig. 1A (A: 5'- GCCTCTGAGGATTTCCTGTGAGG-3'; B: 5'- ATGGAGACCCGCTACAACCT-3'; C: 5'- GCAGGATAATGCTTGGTGGTT-3'). The expected amplicon sizes are 458bp for the wild-type, 531bp for the 'floxed', and 538bp for the knockout allele.

Animals were housed at the Whitehead Institute for Biomedical Research and maintained according to protocols approved by the Massachusetts Institute of Technology Committee on Animal Care.

Cell culture - MEFs were generated from E13.5 fetuses and cultured in DME medium supplemented with 10% IFS, 1 mM glutamine and 10 mM β-mercaptoethanol (MEF medium). In the experiments described here, matched pairs of primary wild type and knock-out MEFs from

littermates were used (except for experiments with SV40, for which we used MEFs that had been immortalized by serial passage).

B cells were isolated from spleens of *Ube2j1*$^{-/-}$ or CD19-Cre *Ube2j1*$^{fl/fl}$ mice and Cre-matched *Ube2j1*$^{WT/WT}$ littermates, respectively. Splenocytes were enriched for B cells by depletion of non-B cells using 'Mouse CD43 Dynabeads' (Life Technologies; Grand Island, NY) according to the manufacturer's protocol. B cells were cultured in Roswell Park Memorial Institute (RPMI) medium with 10% fetal calf serum, 1 mM glutamine, 10mM β-mercaptoethanol and MEM non-essential amino acids (Gibco, Life Technologies; Grand Island, NY) (B cell medium). B plasma cells were induced by adding 1 μM CpG-DNA 1826 (a TLR9 agonist, phosphorothioate backbone, 5'-TCCATGACGTTCCTGACGTT-3'; IDT, Coralville, IA) to the B cell medium for 4 days.

Immunoblotting - Mouse organs were homogenized in PBS containing protease inhibitors (complete protease inhibitor cocktail tablets; Roche Applied Science, Indianapolis, IN) with a rotor-stator homogenizer (TissueRuptor; Qiagen, Gaithersburg, MD). Homogenates were made in PBS containing 1% (v/v) NP-40. MEFs were lysed in PBS with 0.1%. Samples were immunoblotted using standard techniques.

Antibodies for immunoblotting - Antibodies to OS-9 (NB100-519, rabbit polyclonal, 1/1000; Novus Biologicals, Littleton, CO), p97 (10R-P104a, mouse monoclonal, 1/1000; Fitzgerald, Acton, MA), EDEM-1 (affinity-purified rabbit polyclonal, 1/1000; Sigma-Aldrich, St. Louis, MO), Malectin (rabbit polyclonal, 1/1500; Abcam, Cambridge, MA) and HRD-1 (NB100-2526, rabbit polyclonal, 1/1000; Novus Biologicals, Littleton, CO) were obtained commercially. Antibodies to XTP3-B ((8), rabbit polyclonal serum, 1/5000; gift from Ron Kopito, Stanford) and ATF6 ((9), affinity-purified rabbit polyclonal, 1/500; gift from Ronald Wek, University of Indiana) have been described before. Anti-UBE2J1 ((5), rabbit polyclonal serum, 1/4000), anti-gp96 (rabbit polyclonal serum, 1/4000), anti-SEL1L ((10), rabbit polyclonal serum, 1/4000), anti-PDI (rabbit polyclonal serum, 1/4000), UBXD8 ((5), rabbit polyclonal serum, 1/4000), Derlin-1 ((11), rabbit polyclonal serum, 1/4000), Derlin-2 ((11), rabbit polyclonal serum, 1/4000) and YOD1 ((12), affinity-purified rabbit polyclonal, 1/1000) were produced by our laboratory.

Antibodies for FACS analysis - The antibodies used were anti-mouse IgM PE (clone II/41; eBioscience, San Diego, CA), anti-mouse B220 Pacific Blue (clone RA3-6B2; BD Pharmingen, San Jose, CA), anti-mouse AA4.1 (CD93) PerCP-Cy5.5 (clone AA4.1; eBioscience, San Diego, CA), anti-mouse CD1d PE (clone 1B1; eBioscience, San Diego, CA), anti-mouse CD21/CD35 APC (clone 7E9; BioLegend, Inc., San Diego, CA), anti-mouse CD23 FITC (clone B3B4; BD Pharmingen, San Jose, CA), anti-mouse CD19 FITC (clone 1B3; BD Pharmingen, San Jose, CA), anti-mouse CD5 PerCP-Cy5.5 (clone 53-7.3; eBioscience, San Diego, CA) and anti-mouse CD43 PE (clone S7; BD Pharmingen, San Jose, CA).

Pulse-chase analysis - Plasmablasts were analyzed after four days of culture in B cell medium with 1 μM CpG-DNA 1826. Cells were pretreated for five hours with 1 μg/ml tunicamycin (T7765; Sigma-Aldrich, St. Louis, MO) or left untreated, then starved for 1 hour in serum-free RPMI medium followed by a 20 minute labeling period with ^{35}S-cysteine/methione (EXPRE35S35S Protein Labeling Mix, NEG072014MC; PerkinElmer, Inc, Waltham, MA). Aliquots were taken after chase periods of 0, 30, 60 and 120 minutes. The supernatants were saved for immunoprecipitation. Cells were washed once in ice-cold PBS and lysed in NET buffer (50 mM Tris pH7.4, 150 mM NaCl, 0.5% v/v NP-40, 5 mM EDTA) with complete protease inhibitors. Equivalent amounts of radiolabeled proteins were used for immunoprecipitations. IgM was immunoprecipitated with a μ chain-specific goat anti-mouse IgM antibody (1020-01; Southern Biotech, Birmingham, AL). Class I MHC was immunprecipitated with an H-2K^b heavy chain-specific rabbit serum (p8, produced in our laboratory according to (13)).

RNA isolation and RNA-Seq analysis - RNA for the RNA-Seq analysis was isolated from passage three MEFs with an RNeasy Plus Mini Kit according to the manufacturer's protocol. Total RNA was analyzed for integrity with the RNA Pico kit on an Agilent 2100 Bioanalyzer (Agilent Technologies, Santa Clara, CA). Total RNA input amounts for library preparation were normalized and libraries were prepared using the Illumina

TruSeq TM V2 RNA Library Preparation Kit (Illumina, Inc., San Diego, CA) following the manufacturer's protocol with slight modifications in the PCR step. Fifteen cycles of PCR were done using the HiFi NGS Library Amplification kit (KAPA Biosystems, Wilmington, MA). The libraries were quantified by qPCR using the Illumina Library Quantification kit (KAPA Biosystems, Wilmington, MA) according to the manufacturer's protocol and sized using the High Sensitivity DNA kit from Agilent (Agilent Technologies, Santa Clara, CA). The RNA-Seq libraries were sequenced using the Illumina HiSeq 2000 instrument (Illumina, Inc., San Diego, CA) for 40 bases (unidirectional). Sequence as well as quality scores were generated using the Off-Line Basecaller software (version 1.9.4; Illumina, Inc., San Diego, CA). *FACS analysis* - Single cell suspensions of bone marrow cells, splenocytes and peritoneal cavity cells were prepared and red blood cells were lysed. Cell suspensions were adjusted to the same concentration before surface staining in PBS with 2% fetal calf serum. To measure SV40 large T antigen expression, MEFs were fixed and permeabilized. SV40 Large T antigen was stained with a monoclonal mouse anti-SV40 large T antigen antibody ((14); gift from Ari Helenius, ETH Zurich) and goat anti-mouse IgG AlexaFluor647 (A21235; Life Technologies). Samples were analyzed on a BD FACSCalibur or BD LSRII flow cytometer and data were processed using FlowJo software (TreeStar, Ashland, OR).

ER stress induction and analysis - ER stress was induced in MEFs by culturing cells in MEF medium with tunicamycin (T7765; Sigma-Aldrich) at the indicated concentrations. Induction of ER stress was assessed by immunoblotting for ATF6 or RT-PCR for splicing of the XBP-1u mRNA. For the the XBP-1u RT-PCR, RNA from stimulated cells was isolated with an RNeasy mini kit (Qiagen, Gaithersburg, MD) and cDNA was generated by reverse transcription using oligo-dT primers (SuperScript® III First-Strand Synthesis System; Life Technologies). cDNAs of the XBP-1u (unspliced) and XBP-1s (spliced) mRNAs were detected by PCR amplification of a sequence surrounding the excised intron (forward: 5'-GAACCAGGAGTTAAGAACACG-3'; reverse: 5'-AGGCAACAGTGTCAGAGTCC-3').

SV40 assays - SV40 was produced and titrated in simian CV-1 cells and crude virus extracts obtained as described (15). For infection experiments, cells were seeded at a confluency of ~60%. On the day of the experiment cells were washed with PBS and infection medium (RPMI, 3% BSA, 10 mM HEPES pH6.8), then covered with SV40 infection inoculum for 4 hours. Subsequently the inoculum was removed and replaced with MEF medium. Cells were detached with trypsin 16 hours later and fixed for FACS staining of the large T antigen (see above).

In vitro Fertilization (IVF) - Cumulus oocytes complexes (COCs) were isolated from 4-5 weeks old mice, superovulated C57BL/6NTac (Taconic, Hudson, NY) mice. Sperm from Ube2j1$^{-/-}$ mice and wild type littermates were isolated from caudal epididymides. After 10 minutes at 37°C/5% CO_2, sperm cells were video documented, counted and normalized before incubation with COCs. Embryos of different developmental stages were counted once a day for three days. The remaining sperm were spread on glass microscopy slides, fixed for 10 minutes in 100% ethanol and morphologically assessed under a phase contrast microscope.

Analysis of male reproductive organs - Testes and epididymides were fixed in Bouin's solution or 4% paraformaldehyde overnight and then processed into paraffin wax. Periodic acid-Schiff (PAS) stain performed following the manufacturers instructions (Sigma 395B-1KT). For immunohistology, tissues were rehydrated and antigen retrieval was performed in citrate buffer (Spring Bioscience, Pleasanton, CA). After blocking in 10% normal donkey serum, primary antibodies were applied in PBS for 2 h at 37°C. Sections were then washed and immunolocalization was performed with DyLight-conjugated secondary antibodies (Jackson ImmunoResearch Laboratories, West Grove, PA), stained with 50 μg/ml lectin PNA (Molecular Probes) for 5 min and mounted using ProLong Gold with Dapi (Life Technologies). Antibodies used were anti-VASA (AF2030, goat polyclonal, 0.3 μg/ml); R&D biosystems, Minneapolis, MN) and anti-UBE2J1 ((5), rabbit polyclonal serum, 1/200, produced in our laboratory).

Electron microscopy - Testes and epididymides were fixed in 2.5% gluteraldehyde, 3% paraformaldehyde with 5% sucrose in 0.1M

sodium cacodylate buffer (pH 7.4), and post fixed in 1% osmium tetroxide in veronal-acetate buffer. Epididymal sperm cells were embedded in agar prior to further processing. Samples were stained in block overnight with 0.5% uranyl acetate in veronal-acetate buffer (pH6.0), then dehydrated and embedded in Embed-812 resin. 50 nm sections were cut on a Leica Ultracut UCT microtome with a Diatome diamond knife, and stained with uranyl acetate and lead citrate. The sections were examined using a FEI Tecnai Spirit at 80KeV.

RESULTS

Conditional ablation of Ube2j1

We inserted LoxP sites into intron 1 and 3 of the *Ube2j1* gene to allow conditional ablation of *Ube2j1* (Fig. 1A). Correctly targeted ES cell clones were injected into blastocysts and the resulting male chimeras were crossed to FLPe transgenic females to delete the Neo cassette in Exon 3, which is flanked by Frt sites. Whole body knockout mice were obtained by crossing 'floxed' mice to CMV-Cre transgenic animals. Intercrosses of *Ube2j1*$^{+/-}$ animals yielded progeny of all possible genotypes as assessed by PCR. MEFs were generated from fetuses on gestation day E13.5. RNA-Seq analysis confirmed the deletion of specifically exons 2 and 3 (Fig. 1B). Analysis of lysates from *Ube2j1*$^{-/-}$ MEFs showed the complete absence of the UBE2J1 protein as assessed by immunoblot. Levels of UBE2J1 in *Ube2j1*$^{+/-}$ MEFs were reduced by half, indicative of a gene dosage effect (Fig. 1C). The additional bands in the wild type and heterozygous samples with apparent molecular weight of ~30 kDa (asterisk in Fig. 1C) might represent a so-far uncharacterized splice variant of *Ube2j1*. Indeed, exon junction analysis of the RNA-Seq data supported skipping of Exon 7 (data not shown).

Ube2j1$^{-/-}$ mice fail to thrive early after birth

Litters from heterozygous parents were born at the expected Mendelian ratios (Fig. 1D), and the weight of P0.5 pups was similar for wild type, heterozygous and knockout animals (Fig. 1E, top panel). At weaning (P21), approximately half of the knockout animals had died (Fig. 1D), the survivors were smaller in size and weighed significantly less than wild-type animals (Fig. 1E, bottom panel). *Ube2j1*$^{+/-}$ mice had intermediate body weights at P21 (Fig. 1E, bottom panel), concordant with intermediate expression levels of UBE2J1 seen in heterozygous MEFs (Fig. 1C). We identified milk spots one day after birth in both wild type and *Ube2j1*$^{-/-}$ mice, excluding the inability to feed as possible reason for the failure to thrive. We did not observe enhanced mortality in *Ube2j1*$^{-/-}$ animals after weaning. Thus, while the lack of *Ube2j1* does not impair development or growth of embryos in the gestation phase, *Ube2j1* is important for postnatal survival and growth.

Specific components of the ER dislocation machinery are upregulated in the absence of UBE2J1

Removal of key components of a quality control pathway is expected to result in accumulation of misfolded proteins and might therefore activate the unfolded protein response (UPR). However, we did not observe constitutive activation of the UPR in *Ube2j1*$^{-/-}$ MEFs as judged by the splicing status of the *Xbp-1* mRNA (Fig. 3A and 3B), cleavage status of ATF6 (Fig. 3C), and protein (Fig. 2A and B) or transcript levels (Fig. 2D and data not shown) of genes known to be upregulated upon ER stress, unlike what was described in *Derlin-2*$^{-/-}$ MEFs (16). However, when we examined protein levels of ER proteins in MEFs (Fig. 2A) and in lysates prepared from different tissues (Fig 2B and C), we found that OS9, SEL1L and EDEM1 levels were increased in *Ube2j1*$^{-/-}$ MEFs. The observed increase varied with tissue and/or cell-type examined. For example, OS9 was barely detectable in skin from wild type mice, but present at a much higher level in skin from a knockout mouse. While the increase was modest in the large intestine (~2-fold), changes in OS9 levels in MEFs (Fig. 2B), pancreas, thymus and spleen were considerably higher (~5-10-fold, Fig. 2B). Quantitative analysis of RNA-Seq data from MEFs did not show changes similar to those observed in the immunoblots (Fig. 2D and data not shown), implying that increased transcription of the corresponding genes is not the reason for this observation. Regulation at the translational level also seems unlikely, because levels of other proteins, including components of the dislocation machinery such as HRD1, XTP3B, Derlin-1 or Derlin-2, were unaffected (Fig. 2A). The RNA-Seq data confirmed the absence specifically of exons 2 and 3 of *Ube2j1* in *Ube2j1*$^{-/-}$ MEFs (Fig. 1B). Therefore we can conclude with confidence that similar RKPM values for other genes of interest, including those encoding ER quality

control components, reflect similar levels of transcripts.

Taken together, ablation of *Ube2j1* results in the accumulation of specific proteins of the ER quality machinery, probably by their post-translational stabilization.

Ube2j1$^{-/-}$ MEFs are more susceptible to SV40 infection

Having shown upregulation of EDEM1, OS9 and SEL1L in *Ube2j1$^{-/-}$* MEFs, we asked whether there are functional consequences to this remodeling of the ER. ER dislocation components are required for transport of SV40 from the ER to the cytosol (15,17). An increase in the concentration of components involved in ER quality control might therefore facilitate escape of SV40 from the ER. We infected knockout and wild type MEFs with SV40 and quantified infection 20 h later by flow cytometry using antibodies for SV40 large T antigen (TAg). *Ube2j1$^{-/-}$* MEFs were indeed more susceptible to SV40 infection than WT MEFs (Fig 2E). To test whether enhanced susceptibility of *Ube2j1$^{-/-}$* MEFs to infection was not simply due to an increase in the SV40 receptor, the ganglioside GM1, we measured binding of FITC-labeled Cholera Toxin B subunit (FITC-CTxB), which also uses GM1 to bind to cells (18). FITC-CTxB bound equally well to wild-type and knockout MEFs (Fig. 2F). Wild type and *Ube2j1$^{-/-}$* MEFs were equally susceptible to infection with vesicular stomatitis virus (VSV), a virus that does not require ER quality control components for infection (data not shown). SV40 thus infects *Ube2j1$^{-/-}$* MEFs more successfully than wild type MEFs, in agreement with the increased levels of ER quality control components implicated in virus escape from the ER. These components must therefore be properly integrated in the pathway exploited by SV40.

Ube2j1-deficiency does not enhance induction of the unfolded protein response (UPR)

UBE2J1 is one of three E2 ubiquitin conjugating enzymes involved in ER dislocation, and was identified as part of the HRD1-SEL1L complex. We reasoned that its absence might impair the ability of cells to cope with ER stress and thus render cells more susceptible to the UPR. We therefore exposed MEFs to tunicamycin, an inhibitor of N-linked glycosylation that potently induces the UPR. We neither observed differences in the extent of *Xbp-1* splicing (Fig. 3B), nor in the processing of ATF6 (Fig. 3C) in response to tunicamycin treatment. We also did not see differences in response to other inducers of the UPR, such as depletion of ER-resident calcium stores by thapsigargin or by perturbation of redox homeostasis by DTT (data not shown).

Notably, steady-state levels of full-length ATF6 were higher in Ube2j1$^{-/-}$ MEFs (Fig. 3C). ATF6 is itself a substrate that is degraded in a SEL1L-dependent manner (19). Given that mRNA levels of *Atf6* are unaltered in *Ube2j1$^{-/-}$* MEFs (Fig. 2D), it is likely that turnover of ATF6 involves the action of UBE2J1, a component of the SEL1L-containing dislocon, possibly by directly transferring ubiquitin onto dislocated ATF6.

We conclude that *Ube2j1*-deficiency does not render MEFs more susceptible to ER stress.

B cell development, immunoglobulin maturation and immunoglobulin secretion are normal in Ube2j1$^{-/-}$ B cells

The prevailing view is that ER quality control is especially important for tissues and cells with a high secretory load, such as liver, pancreas and B lymphocytes. However, surviving *Ube2j1* knockout mice were seemingly healthy once they reached adulthood. Considering the compensatory mechanism(s) observed in MEFs, we reasoned that a phenotype might be observable only under non-homeostatic conditions or in cells with a high secretory load. We therefore asked if B cell function is affected in the absence of *Ube2j1*.

Ube2j1$^{-/-}$ mice had similar frequencies of immature ($B220^{int}IgM^{+}$), pre-/pro- ($B220^{+}IgM^{-}$) and recirculating ($B220^{hi}IgM^{+}$) B cells in the bone marrow as wild type mice (Fig. 4A). We also observed no difference in frequencies of immature ($B220^{+}AA4.1^{+}$), mature ($B220^{+}AA4.1^{-}$), follicular ($B220^{+}AA4.1^{+}CD21^{lo}CD1d^{lo}$), marginal zone B cell precursors ($B220^{+}AA4.1^{+}CD21^{hi}CD1d^{hi}CD23^{+}$) and marginal zone B cells ($B220^{+}AA4.1^{+}CD21^{hi}CD1d^{hi}CD23^{-}$) in the spleen (Fig. 4A). The average frequencies of total B1 ($B220^{lo}CD19^{+}$), B1a ($B220^{lo}CD19^{+}CD5^{+}$), B1b ($B220^{lo}CD19^{+}CD5^{-}$) and B2 ($B220^{hi}CD19^{+}$) cells in the peritoneal cavity were comparable between *Ube2j1$^{-/-}$* and *Ube2j1$^{+/+}$* control animals (Fig. 4A). We conclude that B cell development is normal in the absence of UBE2J1.

B cells have been used extensively to study the impact of chaperone-dependent protein folding as

well as other aspects of glycoprotein quality control, precisely because of their exceptionally high rates of synthesis, assembly and secretion of immunoglobulins ((20) and references therein). Therefore, we analyzed bulk glycoprotein synthesis and turnover in B cell plasmablasts. Spleens from CD19-Cre *Ube2j1$^{fl/fl}$* and CD19-Cre *Ube2j1$^{wt/wt}$* were enriched for B cells by exclusion of CD43^{+} cells. CD43^{-} cells were then stimulated with 1μM CpG-DNA for four days to obtain B plasmablasts. Plasmablasts were metabolically labeled with ^{35}S-cysteine/methionine and the fate of both intracellular and secreted immunglobulins was followed. Maturation and secretion of immunoglobulin or maturation of the class I MHC molecule H2-K^{b} were indistinguishable between *Ube2j1$^{-/-}$* and control mice (Fig. 4B). Imposition of additional ER stress by exposure of plasmablasts to tunicamycin for 5 hours prior to pulse-chase analysis did not show any differences in stability or secretion of immunoglobulins either (Fig. 4C). In the aggregate, UBE2J1 is required neither for B cell maturation nor is it essential for synthesis, assembly or secretion of immunoglobulins by B plasmablasts. The lack of detectable alterations in the overall composition of serum proteins, produced mostly by the liver, is also consistent with this conclusion (data not shown).

Male Ube2j1-/- mice are sterile

In our attempt to breed *Ube2j1$^{-/-}$* animals we readily obtained litters from *Ube2j1$^{-/-}$* females intercrossed with heterozygous males. In contrast, breeding pairs with male *Ube2j1$^{-/-}$* animals (n=6) produced no offspring. When co-housing individual male *Ube2j1$^{-/-}$* animals overnight with heterozygous females, vaginal plugs were observed, indicating that *Ube2j1$^{-/-}$* males were sexually active, but no pregnancies were observed.

To understand the underlying defect of this observation we first analyzed epididymal sperm. The total numbers of sperm cells isolated from epididymides of *Ube2j1$^{-/-}$* mice were significantly reduced (Fig. 5A). Since the amount of residual sperm might still be sufficient to confer fertility (21,22), we asked if the remaining sperm cells are functional. We found that the motility of spermatozoa isolated from the epididymis was severely impaired in *Ube2j1$^{-/-}$* mice (Fig. 5B, Movie S1) as compared with wild type controls (Fig. 5B, Movie S2), pointing to defects in flagella function. *Ube2j1$^{-/-}$* animals had a strikingly increased frequency of sperm cells with aberrant morphologies (91% vs. 26% normal, 4% vs. 59% with abnormal head morphology, 5% vs. 15% acephalic sperm in wild type vs. *Ube2j1$^{-/-}$* sperm, respectively; Fig. 5C and D). Further, epididymal sperm preparations from *Ube2j1$^{-/-}$* mice contained cell debris (Movie S2). Next, we tested if sperm from *Ube2j1$^{-/-}$* mice could fertilize eggs *in vitro*. We incubated sperm from wild type (Movie S3) or *Ube2j1$^{-/-}$* (Movie S4) mice with eggs from wild type mice. Sperm cells from *Ube2j1$^{-/-}$* mice rarely bound to isolated eggs, consistent with abnormal sperm function and were unable to fertilize eggs. One day after IVF, we observed a single 2-cell embryo with sperm from *Ube2j1$^{-/-}$* animals (n=3 males, ~200 eggs per male), which did not survive to the 4-cell stage. In contrast, ~54% of the eggs fertilized with sperm from wild type males proceeded to the 2-cell stage one day after IVF (n=3 males, ~200 eggs per male). By day 3.5 after IVF, ~36% of the eggs fertilized with control sperm reached the morula stage and ~17% had developed into a blastocyst. In contrast, all eggs that had been incubated with *Ube2j1$^{-/-}$* sperm had died or had not proceeded to the 2-cell stage (Fig. 5E). Given its severely reduced mobility (Movie S2) and impaired ability to bind to the zona pellucida (Movie S4), *Ube2j1$^{-/-}$* sperm most probably did not efficiently fertilize the oocytes, although we cannot formally exclude a defect in the sperm's ability to support post-fertilization embryo development.

Taken together, male *Ube2j1$^{-/-}$* mice are sterile. Their sperm cells are morphologically abnormal, display severely impaired mobility and cannot generate multi-cell embryos in an IVF setting.

Male Ube2j1$^{-/-}$ mice have defects in spermatid development

Considering that *Ube2j1$^{-/-}$* spermatozoa are defective and given that UBE2J1 is highly expressed in testicular extracts (Fig. 2C), we next investigated the role of *Ube2j1* in spermatogenesis. Immunolocalization of UBE2J1 revealed strong expression in the early maturation phase of elongate spermatids between step 12 and 15 (Fig. 6A), a period in which the ER undergoes massive, dynamic changes, as previously described (23). This expression gradually diminished as spermatids reduced their cytoplasmic content, consistent with the regression of the ER at this time (23,24). The specificity of

the staining with the anti-UBE2J1 antibody is validated by the absence of staining in *Ube2j1*$^{-/-}$ testis sections (Fig. 6A, right panel). We did not detect UBE2J1 in meiotic or mitotic germ cells (Fig. 6B).

The expression of UBE2J1 in elongate spermatids in conjunction with reduced epididymal sperm number, motility and morphology in *Ube2j1*$^{-/-}$ mice suggested a defect in the final phases of germ cell maturation. To assess spermatogenesis, we performed periodic acid-Schiff (PAS) stains on testis sections. Mouse spermatogenesis is characterized by a defined set of germ cell associations, by which germ cell stem cells (spermatogonia) differentiate and progress through meiosis and spermiogenesis to produce haploid spermatozoa for fertility. At stage VIII of spermatogenesis, elongate spermatids are released into the tubular lumen in a process known as spermiation (25). Haploid round spermatids, previously located immediately basal to elongate spermatids, then start a dramatic morphological transformation into elongate spermatids from late stage VIII onwards. In this way, only one generation of elongate spermatids is observed at any stage of mouse spermatogenesis (26). In *Ube2j1*$^{-/-}$ mice, we frequently observed abnormal germ cell associations, with retained elongate spermatids from stage IX onwards (Fig. 6C), indicative of defective spermiation (25). These spermatids are subsequently released into the tubular lumen, or phagocytosed by the seminiferous epithelium (asterisks in Fig.6C).

We also observed focal regions of mixed hypospermatogenesis in all *Ube2j1*$^{-/-}$ mice examined (data not shown), indicating that additional spermatogenic defects may contribute to compromised fertility in these males.

The average weights of testes from wild type, heterozygous and *Ube2j1*$^{-/-}$ males were all similar, although we observed substantially smaller testes in a few knockout animals (Fig. 6D).

We conclude that spermatid development is defective in *Ube2j1*$^{-/-}$ mice as manifested by frequent abnormal germ cell associations.

Structural abnormalities in Ube2j1$^{-/-}$ *sperm*

To gain further insight into the defects imposed on spermatids by the lack of *Ube2j1*, we analyzed the ultrastructure of the testis and epididymal sperm by electron microscopy. Fig. 7A shows stage IX spermatids and retained spermatids (asterisks) in a stage IX seminiferous tubule form the testis of a *Ube2j1*$^{-/-}$ mouse. Both spermatids retained in the testis (Fig. 7A) and epididymal sperm cells from *Ube2j1*$^{-/-}$ mice (Fig. 7C, D, F and G) showed the presence of cytoplasm around their acrosome and neck, an abnormality not observed in sperm from wild type testes (Fig. 7B) or epididymides (Fid. 7E and H). This excess cytoplasm contained organelles, such as endoplasmic reticulum and vacuoles surrounded by one or more membranes. The massively condensed ER morphology (Fig. 7D and G) is reminiscent of the 'radial body' described in (23), which is the typical form of appearance of the ER at steps 14-15 of spermatid development. The 'radial body' denotes a condensed, aggregated, glomerulus-like appearance of the ER at the posterior side of the cell (23). We also observed excess residual cytoplasm in the midpiece of *Ube2j1*$^{-/-}$ epididymal sperm (data not shown), a pathological form of cytoplasmic droplets (27). Cytoplasmic droplet in mice are a cellular structure of epididymal sperm implicated in sperm motility and an indicator for normal spermiogenesis (28). Excess residual cytoplasm around the midpiece in *Ube2j1*$^{-/-}$ sperm might confer the instability responsible for the elevated number of acephalic sperm in the sperm smear (Fig. 5C), and defects in flagella function (Movie S2). Acrosome formation and the (9+2) organization of microtubules in the sperm tails seem to be intact. However, the subacrosomal and perinuclear space were often expanded, leading to the detachment of the acrosome from the condensed nucleus (Fig. 7C and F). Together, the EM data suggest that cytoplasm removal cannot be completed in absence of *Ube2j1*. This failure of cytoplasmic remodeling initiates a cascade of events that ultimately leads to infertility.

DISCUSSION

The removal and degradation of misfolded or unwanted ER proteins is a process pivotal to maintain homeostasis in the ER. Here, we characterized mice deficient in the ER-anchored E2 ubiquitin-conjugating enzyme UBE2J1, which is part of an E2/E3 ubiquitin ligase complex that marks substrates destined for extraction from the ER and degradation by the proteasome.

Gestation proceeds normally in *Ube2j1*$^{-/-}$ mice and adult animals look normal and show no aberrant behaviors. Nonetheless, approximately half of

Ube2j1$^{-/-}$ mice die early in life, and surviving adult *Ube2j1*$^{-/-}$ mice have significantly reduced body weight, suggesting that there is a critical period after birth for which a proper level of UBE2J1 is required.

In the absence of *Ube2j1*, specific proteins involved in ER quality control, such as OS9, EDEM1 and Sel1L, are upregulated resulting in higher susceptibility to infection by SV40. Why the levels of some but not other components implicated in ER quality control show an increase is unclear. The amount of such components, perhaps not surprisingly, may be controlled dynamically (29,30), according to the immediate needs of the cell. *In vivo* ablation of *Ube2j1*$^{-/-}$ may thus reveal the existence of a feedback loop in which activation of *Ube2j1* attenuates the levels of OS9, EDEM1 and Sel1L. At present we do not know whether ablation of UBE2J1 directly stabilizes OS9, SEL1L or EDEM1 and proteins in the same functional category, or if, owing to the *Ube2j1* deficiency, unfolded proteins accumulate first and then trigger upregulation or stabilization of the latter proteins. Regardless of the exact sequence of events, the observed compensation does not seem to involve the UPR. These findings point to a remarkable robustness and redundancy within the ER quality control system to restore and/or maintain ER homeostasis.

Notwithstanding the absence of a constitutive activation of the UPR, it is intriguing that ATF6 is stabilized in *Ube2j1*$^{-/-}$ cells. As part of the HRD1/SEL1L complex, UBE2J1 might required for turnover of ATF6, consistent with the recent finding that ATF6 is stabilized in absence of SEL1L (19).

The most striking phenotype observed in *Ube2j1*$^{-/-}$ mice is a profound defect in spermatid differentiation, known as spermiogenesis, resulting in male sterility. The massive morphological changes in the course of spermiogenesis include synthesis of the acrosome, chromatin condensation and elongation of the nucleus, formation of the flagellum and remodeling of membrane-delimited organelles. In the final step, called spermiation, remaining cytoplasm is eliminated from the spermatid, intercellular cytoplasmic bridges between spermatids are disrupted, and the strong adhesions between spermatids and the Sertoli cell (ectoplasmic specializations), with which they intimately interact, are removed to facilitate their release into the lumen of the seminiferous tubule (25). UBE2J1 protein was abundantly present in elongating spermatids, specifically from step 12 to 15 of sperm differentiation (31), peaking at step 14. Spermatids at these differentiation steps are largely transcriptionally inactive (32,33), implying that the transcripts are transcribed earlier, and that translation of the *Ube2j1* (and presumably other) transcripts is de-repressed in elongate spermatids (34). Thus, UBE2J1 is likely required at a critical time within the elongating spermatid itself for successful completion of the final steps of differentiation and spermiation. Crossing *Ube2j1*$^{fl/fl}$ mice with a germ-cell specific (e.g. Stra8-Cre) or a Sertoli cell-specific Cre-deleter strain (e.g. Amh-Cre) may allow us in the future to unequivocally determine the cell-type(s) that is/are responsible for the defect in spermiogenesis.

Pups from *Ube2j1*$^{+/-}$ parents are born at expected Mendelian ratios, suggesting that in heterozygous mice, *Ube2j1*$^{-}$ (haploid) sperm are fully functional. This might be explained by the distribution of cellular contents between cells of a clone derived from one *Ube2j1*$^{+/-}$ spermatogonium via cytoplasmic bridges (35). *Ube2j1* transcripts would thereby be shared between adjacent cells of the syncytium, allowing proper differentiation of both *Ube2j1*$^{+}$ and *Ube2j1*$^{-}$ spermatids.

Why is spermiation not executed correctly in *Ube2j1*$^{-/-}$ testes? Microscopic examination showed aberrant spermatozoa and cellular debris in epididymal sperm preparations. Ultrastructural examination of epididymal sperm by electron microscopy revealed excess residual cytoplasm in the head and midpiece region of spermatozoa. These observations are in line with the notion that *Ube2j1* is critical for cytoplasmic removal during the last steps of spermatid differentiation. Considerable structural changes during spermiogenesis in different organelles, particularly the ER, have been observed by TEM and SEM (23). The structural metamorphosis of the ER starts from a branched network of tubular structures, which are spread evenly throughout the cytoplasm (step 13), over a markedly condensed, glomerular structure (radial body, step 14), to a completely degenerated structure, often aggregated with other organelles (step 15). At step 16, immediately prior to sperm release, the ER is no longer detectable (23). Levels of UBE2J1 are highest *precisely* when the ER is massively

remodeled for eventual elimination (steps 13 to 16). We hypothesize that *Ube2j1* is involved in the aforementioned remodeling process, possibly by marking excess proteins for proteasomal degradation. In the absence of *Ube2j1*, ER luminal proteins that depend on active UBE2J1 for their removal might be trapped in the ER and block further condensation of the ER. This might prevent the cell from completing the necessary removal of cytoplasm, as evidenced by excess residual cytoplasm in the head reagion, accompanied by detached acrosomes, and around the midpiece, probably causing defects in flagella function. Abnormal spermatids are likely sensed by Sertoli cells eventually resulting in the spermatid retention and ultimately, phagocytosis by Sertoli cells. This failure of spermiation likely explains the starkly reduced sperm number in the epididymis.

Although essential for the generation of functional sperm cells, how cytoplasmic removal is accomplished in elongating spermatids and which genes are involved in this process is not well understood. In fact, most genes so far associated with defective cytoplasmic removal encode nuclear proteins, such as transition nuclear proteins (*Tnp1*, *Tnp2*, (36)) and the protamines (*Prm1*, *Prm2*, (37)), none of which are likely to directly participate in cytoplasm removal.

An exception might be *LKB1* (Liver kinase B1), a kinase that is predominantly found in the cytoplasm and membrane fractions. Their phenotype with respect to male infertility is strikingly similar to *Ube2j1$^{-/-}$* mice. However, unlike in *Ube2j1$^{-/-}$* mice, the epididymis is completely filled with cell debris in *LKB1$^{-/-}$* mice, and LKB1 is expressed in both meiotic and post-meiotic cells.

An intriguing case is SPEM1 (spermatid maturation 1), a protein of unknown molecular function, which is expressed exclusively in elongating spermatids between steps 14 and 16, implying a function in cytoplasm removal and/or spermiation (38). Akin to *Ube2j1$^{-/-}$* mice, *SPEM1$^{-/-}$* males (but not females) are sterile and their sperm are ~85% immotile because of severe deformations in the head/neck region, caused by retention of cytoplasmic remnants. The ultrastructural characteristics are strikingly similar to our observations in *Ube2j1$^{-/-}$* sperm (38). SPEM1 interacts with UBQLN1 (ubiquilin 1) at the manchette of elongating spermatids (39). Although it was postulated that UBQLN1 participates in spermiogenesis, *in vivo* support for this is still pending. UBQLN1 and its homologue UBQLN2 form a complex with p97/VCP and erasin, both of which are central components of the ER dislocation machinery (40). UBE2J1, UBQLN1 and SPEM1 may function co-operatively during the removal of cytoplasm from elongating spermatids.

Taken together, we identify *Ube2j1* as a key player in the elongation of spermatids, arguably one of the most extreme examples of structural and morphological reorganization of a cell. The role of *Ube2j1* in this context is unique and non-redundant, since *Ube2j1*'s paralogue *Ube2j2* cannot compensate for the defect in spermiogenesis. *Ube2j1* is, to our knowledge, the first reported gene directly linking the little understood process of cytoplasm removal in elongating spermatids with the ubiquitin-proteasome pathway, adding a new layer of regulation to spermiogenesis. Furthermore, our data define a previously unknown physiological function for ER dislocation, a cellular process, which until recently has been characterized mostly in established cell lines using biochemical assays.

Examination of ER components in mouse models of male fertility might well prove informative to further elucidate the cellular processes that regulate spermiogenesis.

Remarkably, components of the ubiquitin-proteasome pathway, including *Ube2j1*, were amongst the most strongly and significantly differentially regulated genes in human in teratozoospermic sperm (41), suggesting that *Ube2j1's* role in spermiogenesis may be conserved in humans. Considering that the genetic causes underlying spermiogenic failure in men are still largely unknown, *Ube2j1* and other components of this pathway warrant closer examination and might be useful as diagnostic markers for male infertility in humans.

REFERENCES

1. Smith, M. H., Ploegh, H. L., and Weissman, J. S. (2011) Road to ruin: targeting proteins for degradation in the endoplasmic reticulum. *Science* **334**, 1086-1090
2. Claessen, J. H., Kundrat, L., and Ploegh, H. L. (2012) Protein quality control in the ER: balancing the ubiquitin checkbook. *Trends Cell Biol* **22**, 22-32
3. Lester, D., Farquharson, C., Russell, G., and Houston, B. (2000) Identification of a family of noncanonical ubiquitin-conjugating enzymes structurally related to yeast UBC6. *Biochem Biophys Res Commun* **269**, 474-480
4. Lenk, U., Yu, H., Walter, J., Gelman, M. S., Hartmann, E., Kopito, R. R., and Sommer, T. (2002) A role for mammalian Ubc6 homologues in ER-associated protein degradation. *J Cell Sci* **115**, 3007-3014
5. Mueller, B., Klemm, E. J., Spooner, E., Claessen, J. H., and Ploegh, H. L. (2008) SEL1L nucleates a protein complex required for dislocation of misfolded glycoproteins. *Proc Natl Acad Sci U S A* **105**, 12325-12330
6. Younger, J. M., Chen, L., Ren, H. Y., Rosser, M. F., Turnbull, E. L., Fan, C. Y., Patterson, C., and Cyr, D. M. (2006) Sequential quality-control checkpoints triage misfolded cystic fibrosis transmembrane conductance regulator. *Cell* **126**, 571-582
7. Hoch, R. V., and Soriano, P. (2006) Context-specific requirements for Fgfr1 signaling through Frs2 and Frs3 during mouse development. *Development* **133**, 663-673
8. Christianson, J. C., Shaler, T. A., Tyler, R. E., and Kopito, R. R. (2008) OS-9 and GRP94 deliver mutant alpha1-antitrypsin to the Hrd1-SEL1L ubiquitin ligase complex for ERAD. *Nat Cell Biol* **10**, 272-282
9. Teske, B. F., Wek, S. A., Bunpo, P., Cundiff, J. K., McClintick, J. N., Anthony, T. G., and Wek, R. C. (2012) The eIF2 kinase PERK and the integrated stress response facilitate activation of ATF6 during endoplasmic reticulum stress. *Mol Biol Cell* **22**, 4390-4405
10. Lilley, B. N., and Ploegh, H. L. (2005) Multiprotein complexes that link dislocation, ubiquitination, and extraction of misfolded proteins from the endoplasmic reticulum membrane. *Proc Natl Acad Sci U S A* **102**, 14296-14301
11. Lilley, B. N., and Ploegh, H. L. (2004) A membrane protein required for dislocation of misfolded proteins from the ER. *Nature* **429**, 834-840
12. Ernst, R., Mueller, B., Ploegh, H. L., and Schlieker, C. (2009) The otubain YOD1 is a deubiquitinating enzyme that associates with p97 to facilitate protein dislocation from the ER. *Mol Cell* **36**, 28-38
13. Smith, M. H., Parker, J. M., Hodges, R. S., and Barber, B. H. (1986) The preparation and characterization of anti-peptide heteroantisera recognizing subregions of the intracytoplasmic domain of class I H-2 antigens. *Mol Immunol* **23**, 1077-1092
14. Hess, R., Rau, P., Schwab, M., Paetzold, S., Kuther, M., Obert, M., Agostini, H., Haessler, C., Braun, D. G., and Brandner, G. (1994) Covalent immunochemical membrane labeling of viable cells with K698-T708, a simian virus 40 tumor antigen-derived peptide. *Pept Res* **7**, 146-152
15. Geiger, R., Andritschke, D., Friebe, S., Herzog, F., Luisoni, S., Heger, T., and Helenius, A. (2011) BAP31 and BiP are essential for dislocation of SV40 from the endoplasmic reticulum to the cytosol. *Nat Cell Biol* **13**, 1305-1314
16. Dougan, S. K., Hu, C. C., Paquet, M. E., Greenblatt, M. B., Kim, J., Lilley, B. N., Watson, N., and Ploegh, H. L. (2011) Derlin-2-deficient mice reveal an essential role for protein dislocation in chondrocytes. *Mol Cell Biol* **31**, 1145-1159

17. Schelhaas, M., Malmstrom, J., Pelkmans, L., Haugstetter, J., Ellgaard, L., Grunewald, K., and Helenius, A. (2007) Simian Virus 40 depends on ER protein folding and quality control factors for entry into host cells. *Cell* **131**, 516-529
18. Tsai, B., Gilbert, J. M., Stehle, T., Lencer, W., Benjamin, T. L., and Rapoport, T. A. (2003) Gangliosides are receptors for murine polyoma virus and SV40. *EMBO J* **22**, 4346-4355
19. Horimoto, S., Ninagawa, S., Okada, T., Koba, H., Sugimoto, T., Kamiya, Y., Kato, K., Takeda, S., and Mori, K. (2013) The Unfolded Protein Response Transducer ATF6 Represents a Novel Transmembrane-type Endoplasmic Reticulum-associated Degradation Substrate Requiring Both Mannose Trimming and SEL1L Protein. *J Biol Chem* **288**, 31517-31527
20. Feige, M. J., Hendershot, L. M., and Buchner, J. (2010) How antibodies fold. *Trends Biochem Sci* **35**, 189-198
21. Kumar, T. R., Wang, Y., Lu, N., and Matzuk, M. M. (1997) Follicle stimulating hormone is required for ovarian follicle maturation but not male fertility. *Nat Genet* **15**, 201-204
22. Kumar, T. R., Varani, S., Wreford, N. G., Telfer, N. M., de Kretser, D. M., and Matzuk, M. M. (2001) Male reproductive phenotypes in double mutant mice lacking both FSHbeta and activin receptor IIA. *Endocrinology* **142**, 3512-3518
23. Nakamoto, T., and Sakai, Y. (1989) Changes in endoplasmic reticulum during spermiogenesis in the mouse. *Cell Tissue Res* **257**, 279-284
24. Clermont, Y., and Rambourg, A. (1978) Evolution of the endoplasmic reticulum during rat spermiogenesis. *Am J Anat* **151**, 191-211
25. O'Donnell, L., Nicholls, P. K., O'Bryan, M. K., McLachlan, R. I., and Stanton, P. G. (2011) Spermiation: The process of sperm release. *Spermatogenesis* **1**, 14-35
26. Oakberg, E. F. (1956) Duration of spermatogenesis in the mouse and timing of stages of the cycle of the seminiferous epithelium. *Am J Anat* **99**, 507-516
27. Rengan, A. K., Agarwal, A., van der Linde, M., and du Plessis, S. S. (2012) An investigation of excess residual cytoplasm in human spermatozoa and its distinction from the cytoplasmic droplet. *Reprod Biol Endocrinol* **10**, 92
28. Xu, H., Yuan, S. Q., Zheng, Z. H., and Yan, W. (2013) The cytoplasmic droplet may be indicative of sperm motility and normal spermiogenesis. *Asian J Androl* **15**, 799-805
29. Bernasconi, R., and Molinari, M. (2011) ERAD and ERAD tuning: disposal of cargo and of ERAD regulators from the mammalian ER. *Curr Opin Cell Biol* **23**, 176-183
30. Bernasconi, R., Galli, C., Kokame, K., and Molinari, M. (2013) Autoadaptive ER-Associated Degradation Defines a Preemptive Unfolded Protein Response Pathway. *Mol Cell* **52**, 783-793
31. Russell, L. D., R.A. Ettlin, A.P. Sinha Hikim, E.D. Clegg. (1990) *Histological and Histopathological Evaluation of the Testis*, Cache River Press, Clearwater, Florida
32. Steger, K. (1999) Transcriptional and translational regulation of gene expression in haploid spermatids. *Anat Embryol (Berl)* **199**, 471-487
33. Sassone-Corsi, P. (2002) Unique chromatin remodeling and transcriptional regulation in spermatogenesis. *Science* **296**, 2176-2178
34. Gan, H., Cai, T., Lin, X., Wu, Y., Wang, X., Yang, F., and Han, C. (2013) Integrative proteomic and transcriptomic analyses reveal multiple post-transcriptional regulatory mechanisms of mouse spermatogenesis. *Mol Cell Proteomics* **12**, 1144-1157

35. de Rooij, D. G., and Russell, L. D. (2000) All you wanted to know about spermatogonia but were afraid to ask. *J Androl* **21**, 776-798
36. Meistrich, M. L., Mohapatra, B., Shirley, C. R., and Zhao, M. (2003) Roles of transition nuclear proteins in spermiogenesis. *Chromosoma* **111**, 483-488
37. Cho, C., Willis, W. D., Goulding, E. H., Jung-Ha, H., Choi, Y. C., Hecht, N. B., and Eddy, E. M. (2001) Haploinsufficiency of protamine-1 or -2 causes infertility in mice. *Nat Genet* **28**, 82-86
38. Zheng, H., Stratton, C. J., Morozumi, K., Jin, J., Yanagimachi, R., and Yan, W. (2007) Lack of Spem1 causes aberrant cytoplasm removal, sperm deformation, and male infertility. *Proc Natl Acad Sci U S A* **104**, 6852-6857
39. Bao, J., Zhang, J., Zheng, H., Xu, C., and Yan, W. (2010) UBQLN1 interacts with SPEM1 and participates in spermiogenesis. *Mol Cell Endocrinol* **327**, 89-97
40. Lim, P. J., Danner, R., Liang, J., Doong, H., Harman, C., Srinivasan, D., Rothenberg, C., Wang, H., Ye, Y., Fang, S., and Monteiro, M. J. (2009) Ubiquilin and p97/VCP bind erasin, forming a complex involved in ERAD. *J Cell Biol* **187**, 201-217
41. Platts, A. E., Dix, D. J., Chemes, H. E., Thompson, K. E., Goodrich, R., Rockett, J. C., Rawe, V. Y., Quintana, S., Diamond, M. P., Strader, L. F., and Krawetz, S. A. (2007) Success and failure in human spermatogenesis as revealed by teratozoospermic RNAs. *Hum Mol Genet* **16**, 763-773

Acknowledgements - We thank Oktay Kirak designing of the targeting vector, John Jackson for routine mouse genotyping, Prat Thiru from Bioinformatics and Research Computing at the Whitehead Institute for help with RNA-Seq analysis, Ari Helenius, Ron Kopito and Ronald Wek for reagents, the Division of Comparative Medicine at the MIT for support with the IVF experiment, Genome Technology Core at the Whitehead Institute for help with the RNA-Seq experiment, and the mouse ES Cell & Transgenic Facility at the Koch Institute for Integrative Cancer Research at the MIT for ES cell targeting.

FOOTNOTES

This work was supported by the NIH and in part by the Cancer Center Support (core) grant P30-CA14051 from the National Cancer Institute.

[1]To whom correspondence should be addressed: Hidde Ploegh, Whitehead Institute for Biomedical Research, 9 Cambridge Center, Cambridge 02142, MA, USA, Tel.: +1-617-324-2031; Fax: +1-617-452-3566; e-mail: ploegh@wi.mit.edu

[2]The abbreviations used are: ATF6, activating transcription factor 6; AUP1, ancient ubiquitous protein 1; cDNA, complementary DNA; CFTR, cystic fibrosis transmembrane conductance regulator; COC, cumulus oocyte complex; CTxB, cholera toxin subunit B; EDEM1, ER degradation enhancer, mannosidase alpha-like 1; ER, endoplasmic reticulum; ERAD, ER-associated degradation; HCMV, human cytomegalovirus; HRD1, HMG-CoA reductase degradation 1; IFS, inactivated fetal calf serum; IVF, in vitro fertilization; LKB1, liver kinase B1; MEFs, mouse embryonic fibroblasts; MEM, minimal essential medium; OS9, osteosarcoma amplified 9; PAS, Periodic acid–Schiff; PDI, protein disulfide isomerase; Prm1, protamine 1; Prm2, protamine 2; RKPM, reads per kilobase of transcript per million mapped reads; SEL1L, sel-1 suppressor of lin-12-like; SPEM1, spermatid maturation 1; Tag, SV40 large T antige; TCR, T-cell receptor; TEM, transmission electron microscopy; Tnp1, transition nuclear protein 1; Tnp2, transition nuclear protein 2; UBQLN1, ubiquilin 1; UBQLN1, ubiquilin 2; UBXD8, ubiquitin regulatory X domain containing 8; UPR, unfolded protein response; VCP, valosin-containing protein; VSV, vesicular stomatitis virus; Xbp-1, X-box binding protein 1.

FIGURE LEGENDS

FIGURE 1. Generation of *Ube2j1$^{fl/fl}$* mice. *Ube2j1$^{-/-}$* mice fail to thrive after birth.
(A) Scheme of the targeting strategy. LoxP sites were introduced into introns 1 and 3 to allow excision of exons 2 and 3 by Cre recombinase. Circled A, B and C indicate annealing sites for the genotyping primers. (B) Representation of the reads measured for *Ube2j1* by RNA-Seq in representative *Ube2j1$^{+/+}$* (WT) or *Ube2j1$^{-/-}$* (KO) MEF lines (passage 3). The bottom panel depicts the intron/exon structure of *Ube2j1*. (C) Immunoblot of MEF lysates from two individual *Ube2j1$^{+/+}$*, *Ube2j1$^{+/-}$* or *Ube2j1$^{-/-}$* embryos, each. Asterisk, potential splice variant. (D) Frequencies of sex and genotypes of pups from *Ube2j1$^{+/-}$* parents at P0.5 (after birth) and P21 (weaning). (E) Weight of *Ube2j1$^{+/+}$*, *Ube2j1$^{+/-}$* and *Ube2j1$^{-/-}$* mice at age P0.5 (top) and P21 (bottom). *: P<0.05; **: P<0.01; ***: P<0.001; n.s.: P>0.05, as determined by one-way ANOVA with Tukey's Multiple Comparison Test.

FIGURE 2. *Ube2j1$^{-/-}$* MEFs and organs express higher levels of specific ER dislocation components, and *Ube2j1$^{-/-}$* MEFs are more susceptible to SV40 infection.
(A) Immunoblots of several components of the ER quality machinery in two independent *Ube2j1$^{+/+}$* (WT) or *Ube2j1$^{-/-}$* (KO) MEF lines, respectively, show increased levels for specific ER quality control components in *Ube2j1$^{-/-}$* MEFs. (B and C) Protein levels in organ lysates from a *Ube2j1$^{-/-}$* mouse and a wild type littermate. SI: small intestine, LI: large intestine, SG: salivary gland, SM: skeletal muscle, LN: lymph nodes, Epi: epididymis. (D) Transcript levels of select genes involved in the ER stress response and ER dislocation are unaltered in *Ube2j1$^{-/-}$* MEFs. Shown are average reads per kilobase per million mapped reads (RPKM) values as determined by RNA-Seq from two independent MEF cell lines (passage 3) per genotype. (E) Wild type or *Ube2j1$^{-/-}$* MEFs were infected with different MOIs of SV40. 24 hours after infection the expression of the large T antigen was measured by FACS. Shown are mean and standard deviation values of relative percentages of infected cells of three independent experiment. **: P<0.01; ***: P<0.001, as determined by Student's t tests. (F) Binding of Cholera Toxin B subunit (FITC-CTxB) to wild type or *Ube2j1$^{-/-}$* MEFs. Shown are mean MFI values and standard deviation of two wild type or two *Ube2j1$^{-/-}$* MEF lines, respectively, from one representative experiment.

FIGURE 3. *Ube2j1*-deficiency does not enhance induction of the UPR.
(A) Representation of the reads measured for *Xbp-1* by RNA-Seq. Shown are reads from unstimulated *Ube2j1$^{+/+}$* (WT) or *Ube2j1$^{-/-}$* (KO) MEF lines (passage 3). The bottom panel depicts the intron/exon structure of *Xbp-1*. (B) Splicing of the Xbp1-mRNA after exposure of *Ube2j1$^{+/+}$* and *Ube2j1$^{-/-}$* MEFs to tunicamycin as measured by RT-PCR. (B) Proteolytic processing of ATF6 after exposure of *Ube2j1$^{+/+}$* and *Ube2j1$^{-/-}$* MEFs to tunicamycin measured by immunoblotting with an antibody directed to the N-terminus of ATF6.

FIGURE 4. B cell development and antibody secretion are normal in absence of *Ube2j1*.
(A) FACS plots for markers of different B cell populations in the bone marrow, spleen and peritoneal cavity revealed no difference in B cell development in *Ube2j1$^{-/-}$* mice. (B) and (C) Synthesis, maturation and secretion of immunoglobulin does not differ significantly between *Ube2j1$^{+/+}$* and *Ube2j1$^{-/-}$* B cells. Shown are autoradiographs of immunoprecipitates for μ chain of IgM and class I MHC heavy chain from B plasmablast lysates (left column) and supernatants (right column) from a pulse-chase experiment (B) without or (C) with pre-treatment (5h) with tunicamycin.

FIGURE 5. *Ube2j1*-deficiency causes male sterility in mice.
(A) Total number of sperm cells in the epididymis of *Ube2j1$^{+/+}$* (WT) or *Ube2j1$^{-/-}$* (KO) mice. *: P<0.05, as determined by unpaired t test. (B) Progressive motility of *Ube2j1$^{-/-}$* sperm cells is impaired. Shown are average percentages of (black) immotile, (white) non-progressively motile and (grey) progressively motile *Ube2j1$^{+/+}$* (WT) or *Ube2j1$^{-/-}$* (KO) sperm cells (n≈200 per mouse, 3 mice per genotype). (C) Assessment of sperm cell morphology. Average percentages of (black) morphologically normal, (white)

acephalic and (grey) morphologically abnormal sperm cells as observed in an ethanol-fixed sperm smear are shown (n≈200 per mouse, 3 mice per genotype). (D) Photographs of ethanol-fixed *Ube2j1*$^{+/+}$ (WT) or *Ube2j1*$^{-/-}$ (KO) spermatozoa. Note the abnormal head morphology in the knockout sperm. (E) Percentages of embryo stages observed in an IVF experiment one, two and 3.5 days after fertilization. Spermatozoa from *Ube2j1*$^{+/+}$ (WT) or *Ube2j1*$^{-/-}$ (KO) mice (3 mice per genotype) were incubated with wild type oocytes (~200 oocytes per sperm of one male) and embryos at the indicated stages were counted.

FIGURE 6. Male *Ube2j1*$^{-/-}$ mice have defects in spermatid differentiation.
(A) Immunohistochemical staining for UBE2J1 (16), acrosomes (PNA lectin, red) and DNA (DAPI, blue) in testis cross-sections of a wild type mouse. Note the stage-specific expression of UBE2J1. No staining was detected in *Ube2j1*$^{-/-}$ testes (right panel). Scale bar: 10μm. (B) Immunohistochemical staining for UBE2J1 (16) and the germ cell-specific DDX4 (red) in a wild type testis. (C) PAS-stained cross-section of testes from *Ube2j1*$^{+/+}$ (WT, top row) and *Ube2j1*$^{-/-}$ (bottom row) mice. Note the abnormal germ cell associations and spermiation defect at stage IX. Asterisks denote mislocated spermatids. Filled arrowheads: elongated spermatids to be released at the end of stage VIII. Empty arrowheads: next generation round spermatids. (D) Average testis weight in grams *Ube2j1*$^{+/+}$ (WT), *Ube2j1*$^{+/-}$ (HET), and *Ube2j1*$^{-/-}$ (KO) mice. Shown are mean testis weight of individual mice (data points), and overall average with standard deviation. n.s.: P>0.05, as determined by one-way ANOVA with Tukey's Multiple Comparison Test.

FIGURE 7. Electron microscopy reveals structural abnormalities in *Ube2j1*$^{-/-}$ spermatozoa.
(A) Cross sections of a *Ube2j1*$^{-/-}$ stage IX testis shows retained spermatids (asterisks) with cytoplasm (arrows) above a layer of elongate spermatids. ES: ectoplasmic specialization. (B) Wild type elongated spermatids in the testis. (C, D) *Ube2j1*$^{-/-}$ and (E) wild type spermatids in cross sectioned epididymides. (F, G) *Ube2j1*$^{-/-}$ and (H) wild type spermatids isolated from epididymides. *Ube2j1*$^{-/-}$ spermatozoa retain excess cytoplasm around the acrosome and neck region. Note vacuoles (wedges) surrounded by one or more membranes (F), and retained condensed ER ('radial body', insets) in *Ube2j1*$^{-/-}$ spermatozoa (C, D, F, G). Scale bars: (A, B): 2 μm; (C, D, E, F): 500 nm; (G): 100 nm; (H): 500 nm.

A

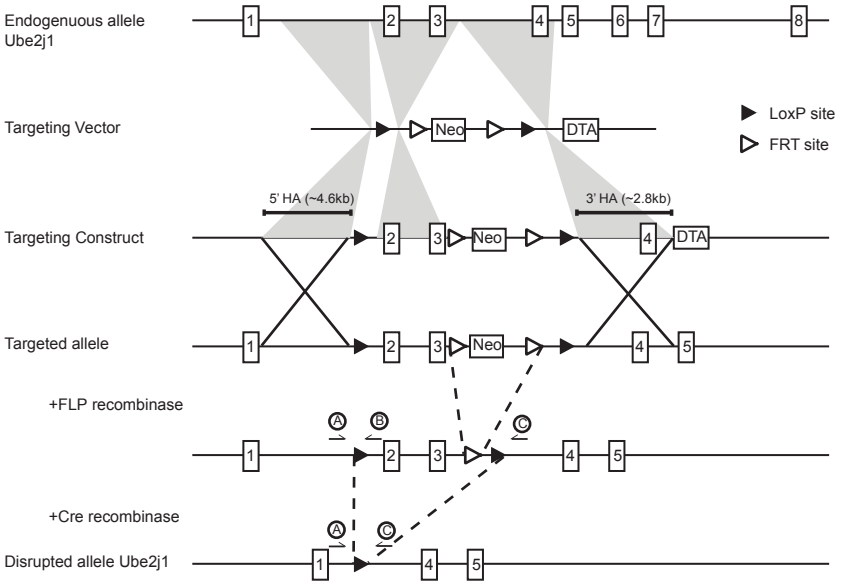

B

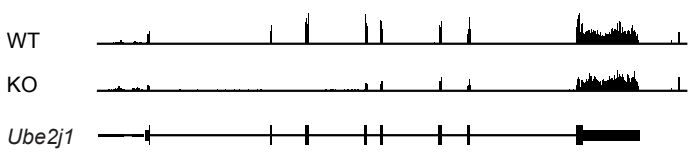

C

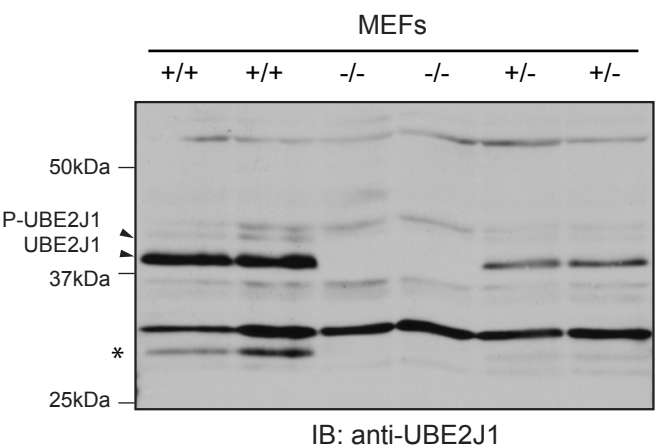

D

	Total	+/+		+/-		-/-	
Mice at P0.5	41	10		21		10	
Frequency P0.5	100%	24%		51%		24%	
		♂	♀	♂	♀	♂	♀
Mice at P21	285	39	35	88	91	15	17
Frequency P21	100%	14%	12%	31%	32%	5%	6%
Expected Frequency	100%	25.0		50.0		25.0	

E

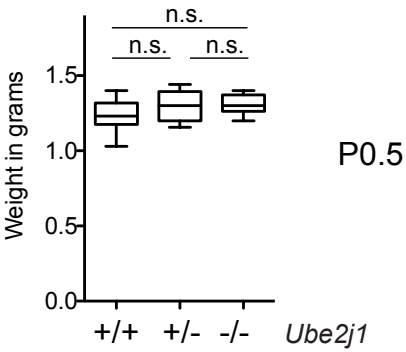

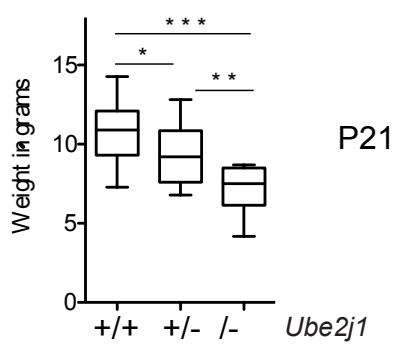

Figure 1

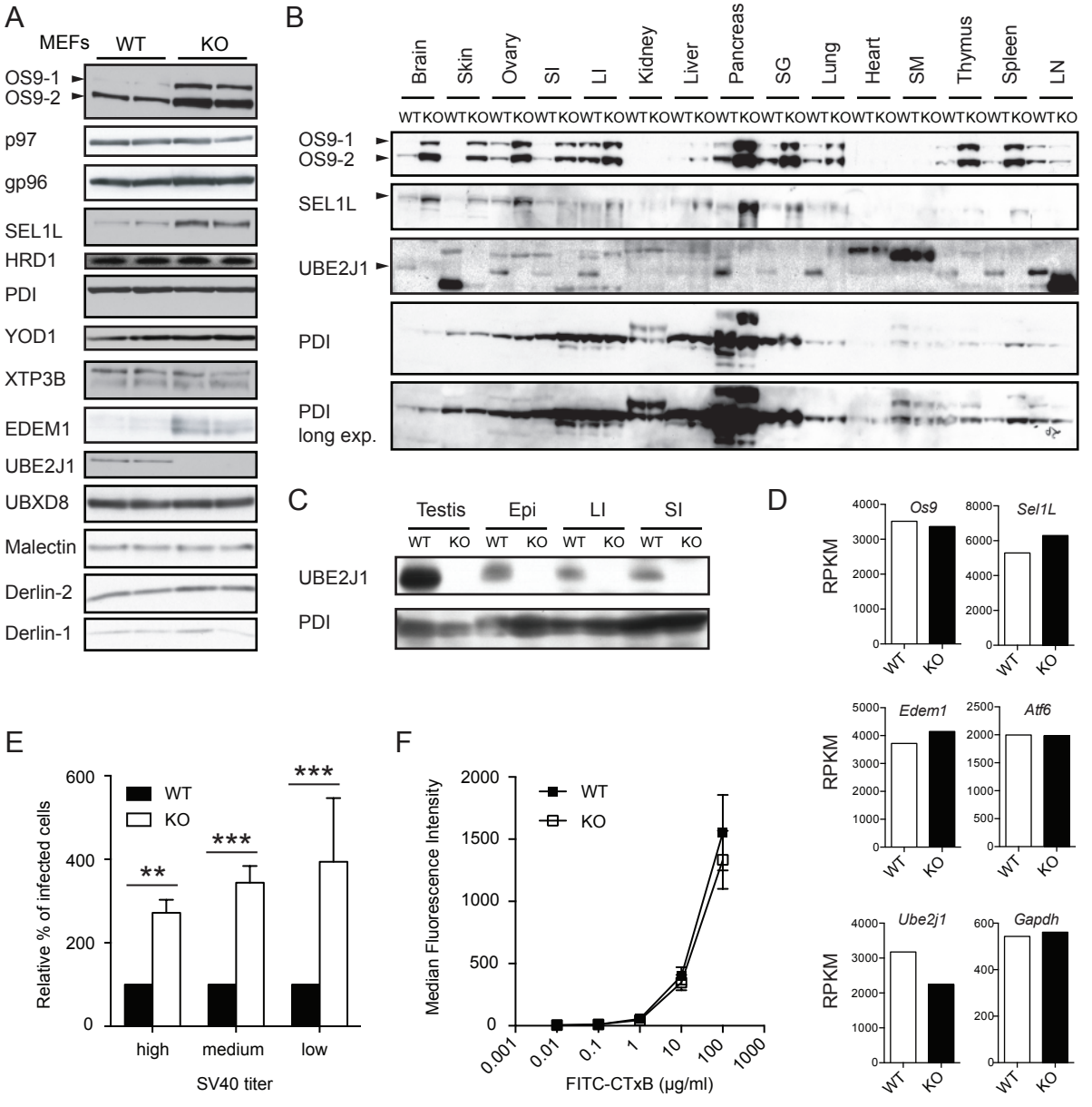
A
MEFs
WT
KO
OS9-1
OS9-2
p97
gp96
SEL1L
HRD1
PDI
YOD1
XTP3B
EDEM1
UBE2J1
UBXD8
Malectin
Derlin-2
Derlin-1
B
Brain
Skin
Ovary
SI
LI
Kidney
Liver
Pancreas
SG
Lung
Heart
SM
Thymus
Spleen
LN
WTKOWTKOWTKOWTKOWTKOWTKOWTKOWTKOWTKOWTKOWTKOWTKOWTKOWTKO
OS9-1
OS9-2
SEL1L
UBE2J1
PDI
PDI
long exp.
C
Testis
Epi
LI
SI
WT KO WT KO WT KO WT KO
UBE2J1
PDI
D
RPKM
Os9
Sel1L
Edem1
Atf6
Ube2j1
Gapdh
WT
KO
E
Relative % of infected cells
WT
KO
**
***
***
high
medium
low
SV40 titer
F
Median Fluorescence Intensity
WT
KO
0.001
0.01
0.1
1
10
100
1000
FITC-CTxB (µg/ml)

Figure 2

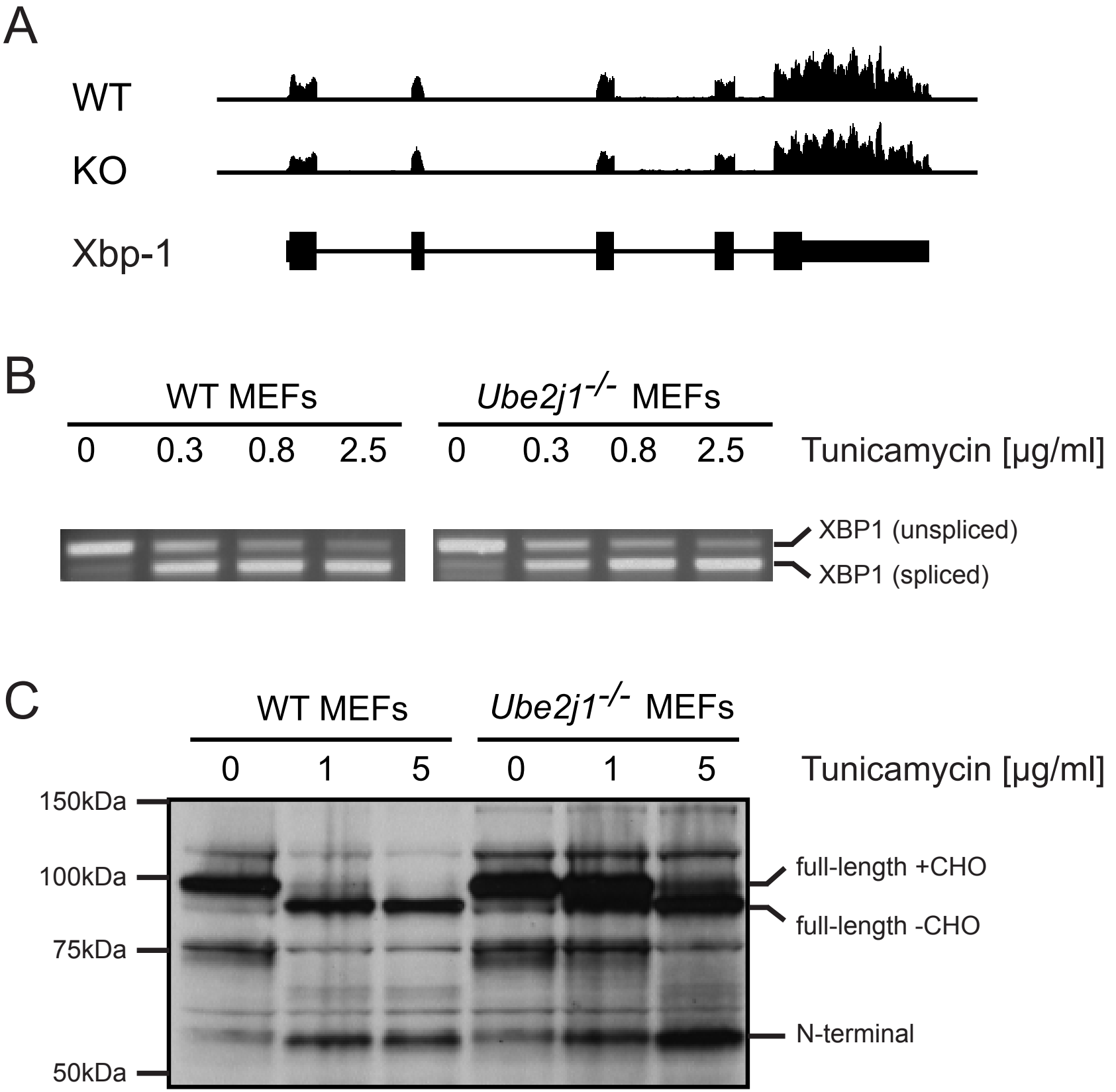
A
WT
KO
Xbp-1
B
WT MEFs
Ube2j1-/- MEFs
0 0.3 0.8 2.5
0 0.3 0.8 2.5
Tunicamycin [μg/ml]
XBP1 (unspliced)
XBP1 (spliced)
C
WT MEFs
Ube2j1-/- MEFs
0 1 5
0 1 5
Tunicamycin [μg/ml]
150kDa
100kDa
75kDa
50kDa
full-length +CHO
full-length -CHO
N-terminal
IB: anti-ATF6

Figure 3

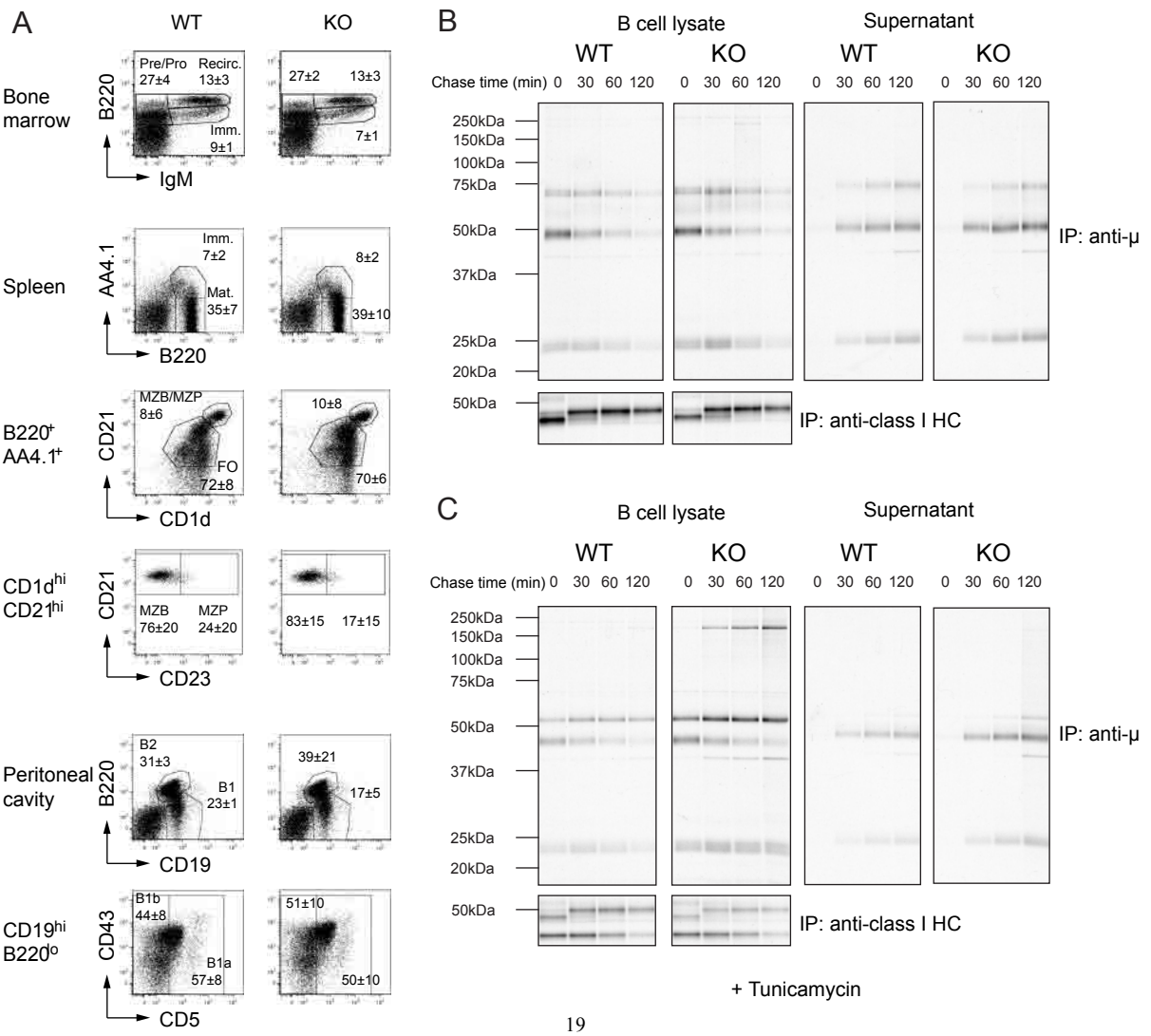
A
WT
KO
Bone marrow
B220
IgM
Pre/Pro 27±4
Recirc. 13±3
Imm. 9±1
27±2
13±3
7±1
Spleen
AA4.1
B220
Imm. 7±2
Mat. 35±7
8±2
39±10
B220+ AA4.1+
CD21
CD1d
MZB/MZP 8±6
FO 72±8
10±8
70±6
CD1dhi CD21hi
CD23
MZB 76±20
MZP 24±20
83±15
17±15
Peritoneal cavity
CD19
B2 31±3
B1 23±1
39±21
17±5
CD19hi B220o
CD43
CD5
B1b 44±8
B1a 57±8
51±10
50±10
B
B cell lysate
Supernatant
WT
KO
Chase time (min) 0 30 60 120
250kDa
150kDa
100kDa
75kDa
50kDa
37kDa
25kDa
20kDa
IP: anti-μ
IP: anti-class I HC
C
+ Tunicamycin

Figure 4

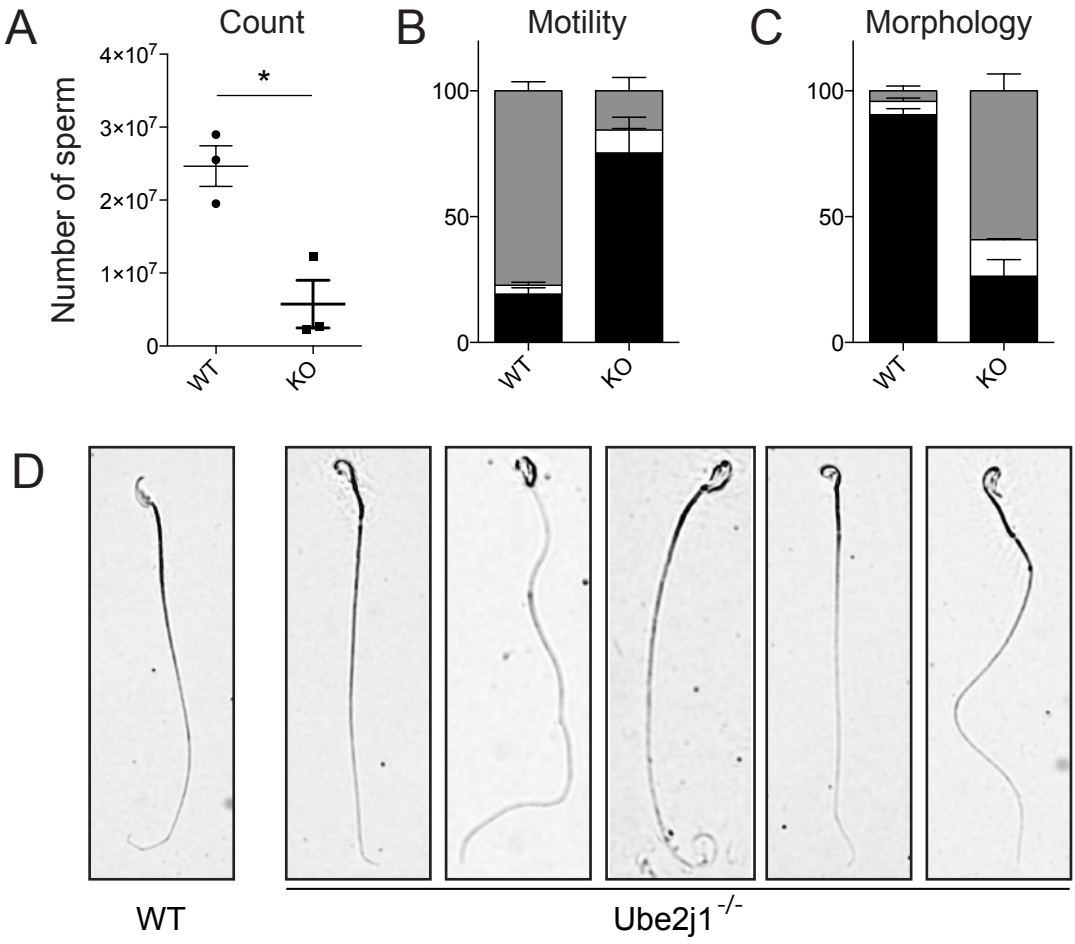

E

	WT	KO	WT	KO	WT	KO
1 cell (oocyte or zygote)	43.8%	98.2%	43.6%	94.7%	37.0%	77.4%
2-cell	53.8%	0.2%	2.2%	0.2%	0.5%	0%
4-cell	0%	0%	32.1%	0%	0.5%	0%
8-cell	0%	0%	20.1%	0%	0%	0%
morula	0%	0%	0%	0%	35.7%	0%
blastocyst	0%	0%	0%	0%	16.6%	0%
dead	2.4%	1.6%	2.0%	5.1%	9.7%	22.6%
	day 1		day 2		day 3.5	

Figure 5

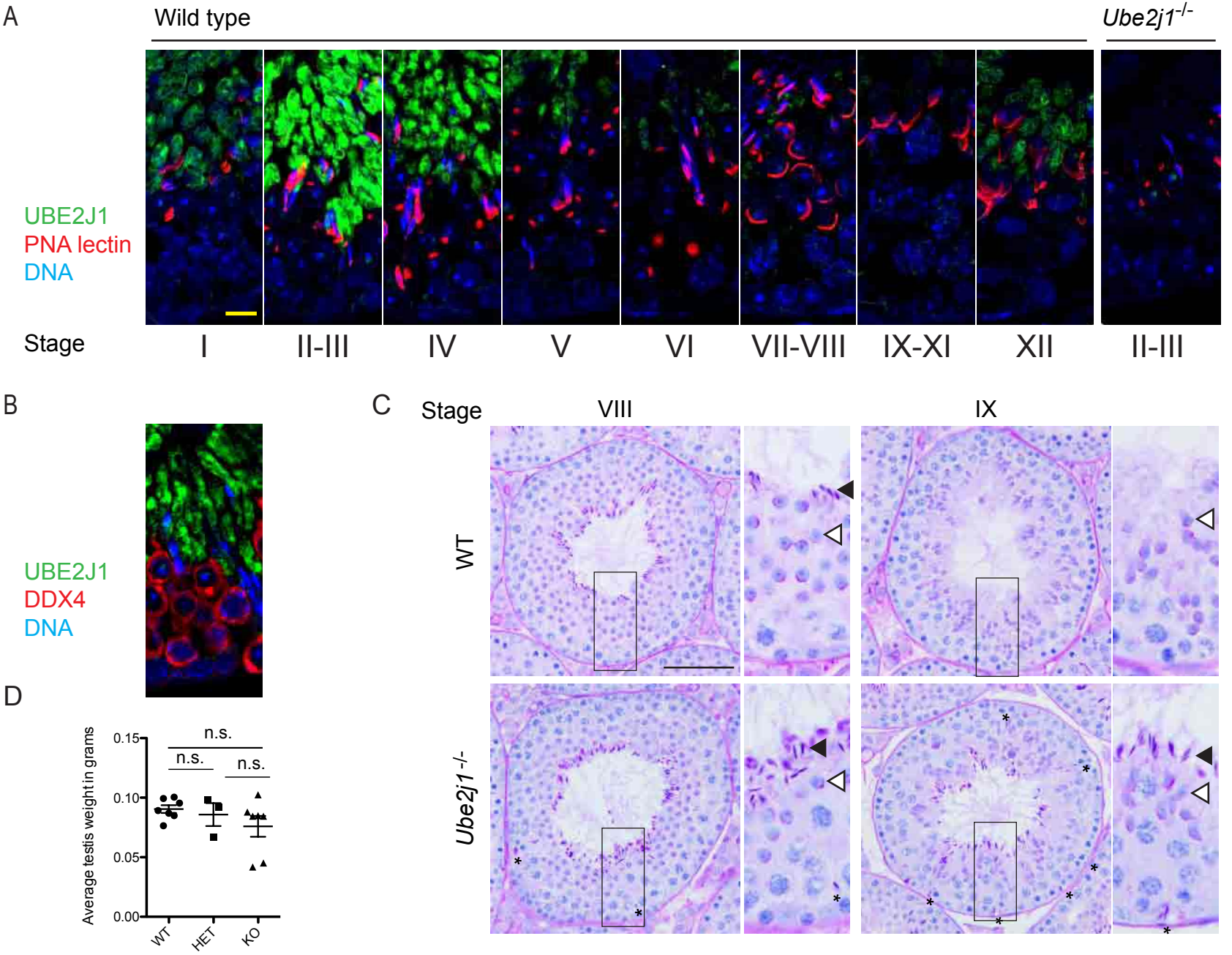
A
Wild type
Ube2j1-/-
UBE2J1
PNA lectin
DNA
Stage
I
II-III
IV
V
VI
VII-VIII
IX-XI
XII
II-III
B
UBE2J1
DDX4
DNA
C
Stage
VIII
IX
WT
Ube2j1 -/-
D
Average testis weight in grams
0.15
0.10
0.05
0.00
n.s.
n.s.
n.s.
WT
HET
KO

Figure 6

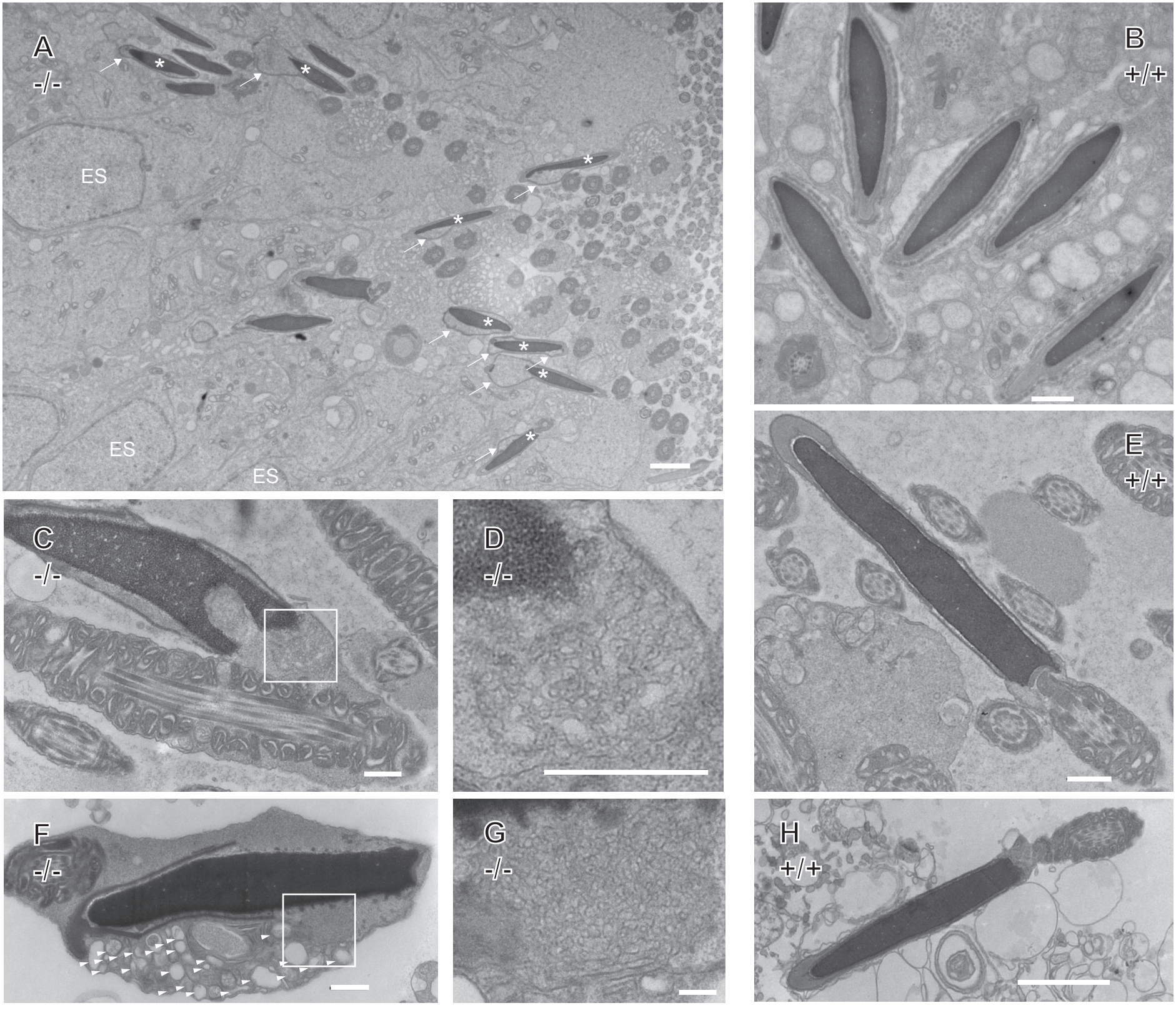

Figure 7